

Visualization of Labeled Mixed-featured Datasets

Yifan Zhu, Fan Dai and Ranjan Maitra

Abstract—We develop methodology for visualization of labeled mixed-featured datasets. We first investigate datasets with continuous features where our Max-Ratio Projection (MRP) method utilizes the group information in high dimensions to provide distinctive lower-dimensional projections that are then displayed using Radviz3D. Our methodology is extended to datasets with discrete and continuous features where a Gaussianized distributional transform is used in conjunction with copula models before applying MRP and visualizing the result using RadViz3D. A R package `radviz3d` implementing our complete methodology is available.

Index Terms—copula models, generalized distributional transform, Indic scripts, principal components, RNA sequences, SVD

I. INTRODUCTION

MODERN applications often yield datasets of many dimensions and complexity. Visualizing such data is important to gain insight into their properties and the similarity or distinctiveness of different groups [1]. However, effective visualization can be challenging because the observations need to be mapped to a lower-dimensional space, with the reduced display conveying information on the characteristics as faithfully as possible. Such displays become even more difficult with mixed-features data, that is, when some of the attributes in the dataset are discrete.

Our major objective in this paper is to visualize high-dimensional datasets with mixed features. Section II-B first develops a Max-Ratio Projection (MRP) method that linearly projects a labeled continuous-features dataset into a lower-dimensional space to allow for its effective visualization via RadViz3D while preserving its group-specific distinctiveness and variability. Our methodology is then extended to provide novel displays of datasets that also have discrete features. Specifically, we use the Gaussianized Distributional Transform (GDT) with copula models to render mixed-features datasets to the continuous space, after which MRP and RadViz3D can be used.

Continuous multivariate data are displayed in many ways [2] (e.g. starplots [3], Chernoff faces [4], parallel coordinate plots [5], [6], surveyplots [7], Andrews’ curves [8], [9], biplots [10], star coordinate plots [11], Uniform Manifold Approximation and Projections (UMAP) [12]). Our paper applies radial visualization or RadViz [13], [14], [15], [16] that projects data onto a circle using Hooke’s law. Here, p -dimensional observations are projected onto the 2D plane using p anchor points equally arranged to be on the perimeter

of a circle. This representation places each observation at the center of the circle that is then pulled by springs in the directions of the p anchor points while being balanced by forces relative to the coordinate values. Observations with similar relative values across all attributes are then placed close to the center while the others are placed closer to anchor points corresponding to the coordinates with higher relative values. However, there is loss of information [17] in RadViz which maps a p -dimensional point to 2D. This loss worsens with increasing p , but can be alleviated by extending it to 3D [18].

Beyond Section II, the paper is organized as follows. Section III illustrates the ability of our methodology to faithfully display labeled data of different separations. Section IV illustrates our methodology on several high-dimensional datasets with mixed features. The main paper concludes with some discussion in Section V. We also have supplementary materials that discuss available methods for displaying high-dimensional datasets, and an online resource at <https://fanne-stat.github.io/RadViz3DExperiments/index.html> that allows for the reader to visualize displays in 3D. Items in the online resource are referenced in this paper with the prefix “S”.

II. METHODOLOGY

A. Visualizing Discrete- and Mixed-Feature Datasets

Datasets with discrete features are complicated to visualize, but arise in genomics, survey and voting preferences and other applications. We develop visualization methods by transforming these datasets using copulas specifically constructed to describe the correlation structure among the discrete variables in the joint distribution while maintaining the empirical marginal distribution. After transformation, we apply multivariate visualization methods. We transform mixed-feature datasets using copulas, for which we introduce the generalized distributional transformation.

Definition 1 (Generalized Distributional Transform, [19], Chapter 1). *Let Y be a real-valued random variable (RV) with cumulative distribution function (CDF) $F(\cdot)$ and let V be a RV independent of Y , such that $V \sim \text{Uniform}(0, 1)$. The generalized distributional transform of Y is $U = F(Y, V)$ where $F(y, \lambda) \doteq P(Y < y) + \lambda P(Y = y) = F(y-) + \lambda\{F(y) - F(y-)\}$ is the generalized CDF of Y , and $F(y-)$ is the left limit of $F(\cdot)$ at y .*

Theorem 2 ([19], Chapter 1). *Let $U = F(Y, V)$ be the distributional transform of Y as per Definition 1. Then*

$$U \sim \text{Uniform}(0, 1) \text{ and } Y = F^{-1}(U) \text{ a.s.}$$

where $F^{-1}(t) = \inf\{y \in \mathcal{R} : F(y) \geq t\}$ is the generalized inverse, or the quantile transform, of $F(\cdot)$.

Y. Zhu and R. Maitra are with the Department of Statistics at Iowa State University, Ames, Iowa 50011, USA. e-mail: {yifanzhu,maitra}@iastate.edu.

F. Dai is with the Department of Mathematical Sciences at the Michigan Technological University, Houghton, Michigan 49931, USA. e-mail: fand@mtu.edu.

Suppose that $\mathbf{Y}_1, \mathbf{Y}_2, \dots, \mathbf{Y}_n$ is a sample of discrete-valued random vectors, each of which has the same distribution as $\mathbf{Y}_1 = (Y_{11}, Y_{12}, \dots, Y_{1p})$, where each margin Y_{1i} has CDF $F_i(\cdot)$ (a step function). Let $U_i = F(Y_{1i}, V_i)$. From Theorem 2, $U_i \sim \text{Uniform}(0, 1)$, so $(U_1, U_2, \dots, U_p) \sim C$ is a copula. Further, from the definition of a quantile transform and Theorem 2, the joint distribution for \mathbf{Y}_1 can be specified in terms of $F_i(\cdot)$ s and the constructed copula C as

$$\begin{aligned} F(y_1, y_2, \dots, y_p) &= \mathbb{P}(Y_{11} \leq y_1, Y_{12} \leq y_2, \dots, Y_{1p} \leq y_p) \\ &= \mathbb{P}[F_i^{-1}(U_i) \leq y_i \forall i = 1, 2, \dots, p] \\ &= \mathbb{P}[U_i \leq F_i(y_i) \forall i = 1, 2, \dots, p] \\ &= C[F_1(y_1), F_2(y_2), \dots, F_p(y_p)]. \end{aligned}$$

Now, we pick p continuous marginal distributions, each with CDF $\tilde{F}_i(\cdot), i = 1, 2, \dots, p$. Then $(\tilde{F}_1^{-1}(U_1), \tilde{F}_2^{-1}(U_2), \dots, \tilde{F}_p^{-1}(U_p))$ has a continuous joint distribution with marginals $\tilde{F}_i(\cdot), i = 1, 2, \dots, p$, and the copula associated with this joint distribution is also C .

We use the marginal empirical CDF (ECDF) $\hat{F}_i(\cdot)$ of the \mathbf{Y}_j s to estimate $F_i(\cdot)$ for $i = 1, 2, \dots, p$. We use $\mathcal{N}(0, 1)$ as the continuous marginals, i.e. $\tilde{F}_i(\cdot) = \Phi(\cdot)$, the $N(0, 1)$ CDF. We define the Gaussianized distributional transform (GDT)

$$G(\mathbf{Y}_j, \mathbf{V}_j) \doteq [[\Phi^{-1}(\hat{F}_i(Y_{ji}, V_{ji}))]]_{i=1,2,\dots,p} \quad (1)$$

for $j = 1, 2, \dots, n$. Here $\mathbf{V}_j = (V_{j1}, V_{j2}, \dots, V_{jp})$, and V_{ji} s are independent identically distributed standard uniform realizations. Then $\mathbf{X}_i = G(\mathbf{Y}_i, \mathbf{V}_i), i = 1, 2, \dots, n$ are realizations from a distribution on \mathcal{R}^p : we apply the methods of Section II-B on $\mathbf{X}_1, \mathbf{X}_2, \dots, \mathbf{X}_n$ before visualizing the resulting MRPs using RadViz3D.

Remark 3. We make a few comments on our use of the GDT:

- 1) For a continuous random variable, Theorem 2 reduces to the usual CDF so $G(\cdot, \cdot)$ can be applied also to datasets with mixed (continuous and discrete) features.
- 2) The GDT is a more stringent standardization than the usual affine transformation that only sets a dataset to have zero mean and unit variance, because it transforms the marginal ECDFs to $\Phi(\cdot)$. So the GDT may, also be applied to datasets with skewed continuous features.
- 3) When datasets have discrete features with little class-discriminating ability, applying the GDT on such features will inflate the variance in the transformed space, resulting in a standard normal coordinate that is independent of the other features. When the number of such coordinates is substantial relative to group-discriminating features, these independent $\mathcal{N}(0, 1)$ -transformed coordinates will drive the MRP, resulting in poor separation. So we use an analysis of variance (ANOVA) test on each copula-transformed coordinate to ascertain if it contains significant group-discriminating information. Multiple significance issues are addressed by correcting for false discoveries [20]. Features so ascertained to not have significant discriminating information are dropped from the MRP and subsequent steps.

B. Visualizing High-dimensional Datasets

With the machinery for GDT in place, we now investigate methods for summarizing labeled high-dimensional data with mixed features. For even moderate dimensions ($p > 10$), displaying many coordinates is not helpful even after factoring in the benefits of going to 3D. So we project our high-dimensional datasets into a lower-dimensional space such that the projected coordinates are almost uncorrelated. A common approach to finding uncorrelated projections is Principal Components Analysis (PCA) that finds the mutually orthogonal projections summarizing a proportion of the total variance in the data. We propose using PCA for unlabeled data. For labeled data, approaches beyond PCA that exploit class labels [21] are desired. Our objective is to find an approach that preserves the distinctiveness of group labels when finding projections while also preserving, in the display, the inherent variability in the dataset. We develop Max-Ratio Projections (MRPs) of the data that maximizes separation between groups (in projected space) relative to its total variability. We discuss obtaining these projections next.

a) Directions that Maximize Between-Group Variance: Given a labeled dataset, we find a linear subspace such that the groups are well-separated when the data are projected along this subspace. Let $\mathbf{v}_1, \mathbf{v}_2, \dots, \mathbf{v}_k$ be k uncorrelated direction vectors spanning the linear subspace. In order to separate the groups, we want to project the data to each \mathbf{v}_j such that the ratio of the projected between-group sum of squares and the total corrected sum of squares is maximized (equivalently, the ratio of the projected within-group sums of squares and the total corrected sum of squares is minimized).

Let $\Xi = \{\mathbf{X}_1, \mathbf{X}_2, \dots, \mathbf{X}_n\}$ be n p -dimensional observation vectors. Then the corrected total sum of squares and cross-products (SSCP) matrix is $\mathbf{T} = (n-1)\hat{\Sigma}$ where $\hat{\Sigma}$ is the sample dispersion matrix of Ξ . Let $\text{Var}(\mathbf{X}_i) = \Sigma$, then for any projection vector \mathbf{v}_j , we have $\text{Var}(\mathbf{v}_j' \mathbf{X}_i) = \mathbf{v}_j' \Sigma \mathbf{v}_j$. Further, for any two \mathbf{v}_j and \mathbf{v}_l , $\text{Cor}(\mathbf{v}_j' \mathbf{X}_i, \mathbf{v}_l' \mathbf{X}_i) \propto \mathbf{v}_j' \Sigma \mathbf{v}_l = 0$ since the direction vectors decorrelate the observed coordinates. (We may replace Σ with $\hat{\Sigma}$ in the expressions above.) Therefore, we obtain $\mathbf{v}_1, \mathbf{v}_2, \dots, \mathbf{v}_k$ in sequence to satisfy

$$\begin{aligned} \max_{\mathbf{v}_1} \frac{SS_{\text{group}}(\mathbf{v}_1)}{SS_{\text{total}}(\mathbf{v}_1)} \\ \max_{\mathbf{v}_j} \frac{SS_{\text{group}}(\mathbf{v}_j)}{SS_{\text{total}}(\mathbf{v}_j)} &\ni \mathbf{v}_j' \mathbf{T} \mathbf{v}_i = 0, 1 \leq i < j \leq k \end{aligned} \quad (2)$$

where $SS_{\text{total}}(\mathbf{v}_l)$ is the corrected total sum of squares of the data projected along \mathbf{v}_l (so is a scalar quantity), and $SS_{\text{group}}(\mathbf{v}_l)$ is the corrected between-group sum of squares of the data projected along \mathbf{v}_l . Equivalently, if $SS_{\text{within}}(\mathbf{v}_l)$ is the corrected within-group sum of squares of data projected along \mathbf{v}_l , we know $SS_{\text{total}}(\mathbf{v}_l) = SS_{\text{group}}(\mathbf{v}_l) + SS_{\text{within}}(\mathbf{v}_l)$. Therefore the ratio can be written as

$$\frac{SS_{\text{within}}(\mathbf{v}_l)}{SS_{\text{total}}(\mathbf{v}_l)} = 1 - \frac{SS_{\text{group}}(\mathbf{v}_l)}{SS_{\text{total}}(\mathbf{v}_l)}.$$

Then the equivalent form of the optimization problem is

$$\begin{aligned} \min_{\mathbf{v}_1} \frac{SS_{within}(\mathbf{v}_1)}{SS_{total}(\mathbf{v}_1)} \\ \min_{\mathbf{v}_j} \frac{SS_{within}(\mathbf{v}_j)}{SS_{total}(\mathbf{v}_j)} \quad \ni \quad \mathbf{v}'_j \mathbf{T} \mathbf{v}_i = 0, 1 \leq i < j \leq k. \end{aligned} \quad (3)$$

Theorem 4. Max-Ratio Projections. Let $\mathbf{X}_1, \mathbf{X}_2, \dots, \mathbf{X}_n$ be p -dimensional observations from G groups. Let \mathbf{T} be the total corrected SSCP and \mathbf{B} be the corrected SSCP between groups. Let \mathbf{T} and \mathbf{B} both be positive definite. Then

$$\hat{\mathbf{v}}_j = \frac{\mathbf{T}^{-\frac{1}{2}} \hat{\mathbf{w}}_j}{\|\mathbf{T}^{-\frac{1}{2}} \hat{\mathbf{w}}_j\|}, \quad j = 1, 2, \dots, k \quad (4)$$

satisfies (2) where $\hat{\mathbf{w}}_j, j = 1, 2, \dots, k$ are the eigenvectors corresponding to the k largest eigenvalues of $\mathbf{T}^{-1/2} \mathbf{B} \mathbf{T}^{-1/2}$.

Proof. Let $\Gamma_g, g = 1, 2, \dots, G$ be the $n_g \times n$ matrix that selects observations from the matrix \mathbf{X} that has \mathbf{X}_i as its i th row. Here n_g is the number of observations from the g th group, for $g = 1, 2, \dots, G$. Then $\Gamma_g \mathbf{X}$ is the matrix with observations from the g th group in its rows and

$$\mathbf{B} = \mathbf{X}' \left(\sum_{g=1}^G \frac{1}{n_g} \Gamma'_g \mathbf{1}_{n_g} \mathbf{1}'_{n_g} \Gamma_g - \frac{1}{n} \mathbf{1}_n \mathbf{1}'_n \right) \mathbf{X} \quad (5)$$

and $\mathbf{T} = \mathbf{X}' (\mathbf{I}_n - \mathbf{1}_n \mathbf{1}'_n / n) \mathbf{X}$. Also, \mathbf{X} projected along any direction \mathbf{v} yields $SS_{group}(\mathbf{v}) = \mathbf{v}' \mathbf{B} \mathbf{v}$ and $SS_{total}(\mathbf{v}) = \mathbf{v}' \mathbf{T} \mathbf{v}$ so that finding (2) is equivalent to

$$\begin{aligned} \max_{\mathbf{v}_1} \frac{\mathbf{v}'_1 \mathbf{B} \mathbf{v}_1}{\mathbf{v}'_1 \mathbf{T} \mathbf{v}_1} \\ \max_{\mathbf{v}_j} \frac{\mathbf{v}'_j \mathbf{B} \mathbf{v}_j}{\mathbf{v}'_j \mathbf{T} \mathbf{v}_j} \quad \mathbf{v}'_j \mathbf{T} \mathbf{v}_i = 0, 1 \leq i < j \leq k. \end{aligned} \quad (6)$$

Let $\mathbf{w}_j = \mathbf{T}^{1/2} \mathbf{v}_j, j = 1, 2, \dots, k$. Then for each j ,

$$\frac{SS_{group}(\mathbf{v}_j)}{SS_{total}(\mathbf{v}_j)} = \frac{\mathbf{v}'_j \mathbf{B} \mathbf{v}_j}{\mathbf{v}'_j \mathbf{T} \mathbf{v}_j} = \frac{\mathbf{w}'_j \mathbf{T}^{-\frac{1}{2}} \mathbf{B} \mathbf{T}^{-\frac{1}{2}} \mathbf{w}_j}{\mathbf{w}'_j \mathbf{w}_j}$$

and $\mathbf{v}'_j \mathbf{T} \mathbf{v}_i = \mathbf{w}'_j \mathbf{w}_i$. Then, instead of (6), we can sequentially solve the following, with respect to $\mathbf{w}_1, \mathbf{w}_2, \dots, \mathbf{w}_k$:

$$\begin{aligned} \max_{\mathbf{w}_1} \frac{\mathbf{w}'_1 \mathbf{T}^{-\frac{1}{2}} \mathbf{B} \mathbf{T}^{-\frac{1}{2}} \mathbf{w}_1}{\mathbf{w}'_1 \mathbf{w}_1} \\ \max_{\mathbf{w}_j} \frac{\mathbf{w}'_j \mathbf{T}^{-\frac{1}{2}} \mathbf{B} \mathbf{T}^{-\frac{1}{2}} \mathbf{w}_j}{\mathbf{w}'_j \mathbf{w}_j} \quad \ni \quad \mathbf{w}'_j \mathbf{w}_i = 0, 1 \leq i < j \leq k. \end{aligned} \quad (7)$$

$\mathbf{T}^{-\frac{1}{2}} \mathbf{B} \mathbf{T}^{-\frac{1}{2}}$ is nonnegative definite, with at most $G - 1$ positive eigenvalues, so $k \leq G - 1$ in (7). Its eigenvectors $\hat{\mathbf{w}}_1, \hat{\mathbf{w}}_2, \dots, \hat{\mathbf{w}}_k$ (corresponding to its k largest eigenvalues in decreasing order) solve (7). Let $\hat{\mathbf{v}}_j$ be the normalized version of $\mathbf{T}^{-\frac{1}{2}} \hat{\mathbf{w}}_j$. Then $\hat{\mathbf{v}}_j$ s satisfy (6). The theorem follows. \square

Theorem 4 provides the projections that maximize separation between the groups in a lower-dimensional space in a way that also decorrelates the coordinates. The number of projections is limited by $G - 1$. So, for $G \leq 3$, 1 to 2 projections and therefore 1D or 2D displays should be enough. (For $G = 3$, a RadViz2D figure should normally suffice, but, as

we show later in our examples, choosing 4 projections yields a better display even though the additional $4 - G + 1$ projections yield no additional information on group separation. We use springs to provide a physical interpretation for why these additional $4 - G + 1$ coordinates are beneficial. The first $G - 1$ MRP coordinates pull the data with different forces along the corresponding anchor points in a way that permits maximum separation of the classes. The remaining $4 - G + 1$ anchor points correspond to the zero eigenvalues and do not contribute to the separation between groups, and so each group is pulled with equal force in the direction of these anchor points. These additional pulls separate the groups better in RadViz3D than in RadViz2D. (We choose 4 MRPs when $G \leq 4$ for RadViz3D because a 3D sphere is best separated using 4 equi-spaced anchor points because every axis is then equidistant to the other.)

The eigenvalue decomposition of $\mathbf{T}^{-\frac{1}{2}} \mathbf{B} \mathbf{T}^{-\frac{1}{2}}$ assumes a positive definite \mathbf{T} , for which a sufficient condition is that $n_g > p$ for all g . This assumption may not always hold so we now propose to reduce the dimensionality of the dataset for the cases where $p \geq \min_g n_g$ while also preserving as far as possible its group-specific features and variability.

b) Nearest Projection Matrix to Group-Specific Principal Components (PCs): Our approach builds on standard PCA whose goal, it may be recalled, is to project a dataset onto a lower-dimensional subspace in a way that captures most of its total variance. We use projections that summarize the variability within each group. So, we summarize each group by obtaining PCs separately and then finding the closest projection matrix to all the group-specific PCs. Specifically, we have the following

Result 5. Suppose that $\mathbf{V}_1, \mathbf{V}_2, \dots, \mathbf{V}_m$ are $p \times q$ matrices with $\mathbf{V}'_j \mathbf{V}_j = \mathbf{I}_q$, where \mathbf{I}_q is the $q \times q$ identity matrix. Let $\mathbf{V} = \sum_{j=1}^m \mathbf{V}_j$ with singular value decomposition (SVD) $\mathbf{V} = \mathbf{P}_\bullet \mathbf{\Lambda}_\bullet \mathbf{Q}'$ where \mathbf{P}_\bullet is a $p \times q$ matrix of orthogonal columns, \mathbf{Q} is a $q \times q$ orthogonal matrix and $\mathbf{\Lambda}_\bullet$ is a $q \times q$ diagonal matrix with v non-zero entries where $v = \text{rank}(\mathbf{V})$. Then the $p \times q$ matrix $\mathbf{W} = \mathbf{P}_\bullet \mathbf{Q}'$ satisfies

$$\mathbf{W} = \text{argmin} \left\{ \sum_{j=1}^m \|\mathbf{W} - \mathbf{V}_j\|_F^2 : \mathbf{W}' \mathbf{W} = \mathbf{I}_q \right\}. \quad (8)$$

Proof. (Several proofs for Result 5 [22] exist but we provide a novel alternative proof to add to the literature.) Minimizing $\sum_{j=1}^m \|\mathbf{W} - \mathbf{V}_j\|_F^2$ is the same as maximizing $\sum_{j=1}^m \text{trace}(\mathbf{W}' \mathbf{V}_j)$ or, equivalently, $\text{trace}(\mathbf{W}' \mathbf{V})$. Let the full SVD of $\mathbf{V} = [\mathbf{P}_\bullet, \mathbf{P}_o][\mathbf{\Lambda}_\bullet, \mathbf{0}'] \mathbf{Q}'$, where the i th diagonal element of $\mathbf{\Lambda}_\bullet$ is the nonnegative eigenvalue λ_i . Then $\text{trace}(\mathbf{W}' \mathbf{V}) = \text{trace}(\mathbf{Q}' \mathbf{W}' [\mathbf{P}_\bullet, \mathbf{P}_o][\mathbf{\Lambda}_\bullet, \mathbf{0}']')$. Let $\mathbf{B} = \mathbf{Q}' \mathbf{W}' [\mathbf{P}_\bullet, \mathbf{P}_o]$ have b_{ij} as its (i, j) th entry. Then $\mathbf{B} \mathbf{B}' = \mathbf{I}_q$ and $|b_{ij}| \leq 1$ for all i, j . So, $\text{trace}(\mathbf{W}' \mathbf{V}) \leq |\text{trace}(\mathbf{W}' \mathbf{V})| = |\sum_{i=1}^v \lambda_i b_{ii}| \leq \sum \lambda_i |b_{ii}| \leq \sum \lambda_i = \text{trace}(\mathbf{\Lambda}_\bullet)$, with equality holding when $\mathbf{W} = \mathbf{P}_\bullet \mathbf{Q}'$. \square

Result 5 reduces dimensionality of a dataset for when the number of features is larger than the minimum number of records in any group. We take $m = \min\{p, n_1, n_2, \dots, n_g\}$. The k MRPs of our dataset are displayed using RadViz3D.

The choice of k may be based on the clarity of the display, or by the cumulative proportion (we use 90%) of the eigenvalues of $\mathbf{T}^{-1/2}\mathbf{B}\mathbf{T}^{-1/2}$.

Remark 6. We compare MRP with orthogonal linear discriminant analysis (OLDA) [23] and uncorrelated linear discriminant analysis (ULDA) [24]. OLDA also produces orthogonal discriminant vectors that project data onto a lower-dimensional subspace, however the projection vectors satisfy $\mathbf{v}'_i\mathbf{v}_j = 0, i \neq j$. This does not necessarily mean uncorrelated projections of the data since $\mathbf{v}'_j\Sigma\mathbf{v}_i$ is not necessarily zero. In our visualization, $\mathbf{v}'_i\Sigma\mathbf{v}_j = 0, i \neq j$ is desired and MRP satisfies this by producing uncorrelated projection directions. On the other hand, ULDA uses the same set of uncorrelated projection directions as MRP. However, MRP uses the normalized vectors (columns of projection matrix) with unit length, while the column vectors of the ULDA projection matrix are not normalized. Specifically, both ULDA and MRP have $\mathbf{v}'_i\Sigma\mathbf{v}_j = 0, i \neq j$, but in ULDA, $\mathbf{v}'_i\Sigma\mathbf{v}_i = 1$, while in MRP, $\mathbf{v}'_i\mathbf{v}_i = 1$. So the ULDA is actually MRP with a scaling step after the projection, such that each coordinate's variance is 1. In that sense, MRP can display a better visualization as the variance of for each projection direction is preserved.

Algorithm 1 summarizes the use of GDT and MRP for mixed-features datasets.

Algorithm 1 RadViz3D for datasets with mixed features

- 1: Calculate the marginal ECDF $\hat{F}_1(\cdot), \hat{F}_2(\cdot), \dots, \hat{F}_p(\cdot)$ for each of the p coordinates of the dataset.
 - 2: Simulate $\mathbf{V}_i \stackrel{iid}{\sim} \text{Uniform}[0, 1]^p$.
 - 3: Construct the transform $G(\cdot, \cdot)$ with marginal ECDFs and simulated $\mathbf{V}_i, i = 1, 2, \dots, n$, as in Equation 1.
 - 4: Transform \mathbf{Y}_i in the discrete dataset to \mathbf{X}_i with $\mathbf{X}_i = G(\mathbf{Y}_i, \mathbf{V}_i), i = 1, 2, \dots, n$.
 - 5: Apply MRP on $\mathbf{X}_i, i = 1, 2, \dots, n$ via Algorithm 1.
 - 6: Display MRP results by RadViz3D.
-

III. ILLUSTRATIVE PERFORMANCE EVALUATIONS

We illustrate our methodology on simulated 100D datasets of $n = 500$ observations from five groups with both discrete and continuous features and of known group separation and clustering complexity. The MIXSIM package [25] in R [26] allows for the simulation of (continuous) class data according to a pre-specified *generalized overlap* ($\tilde{\omega}$) [27], [28] that indexes clustering complexity, with very small values ($\tilde{\omega} = 0.001$) implying very good separation between groups and larger values ($\tilde{\omega} = 0.05$) indicating poorer separation and increased overlap. We discretize the first 50 coordinates in each group into 10 classes, based on the marginal deciles of the coordinate. We use the GDT and MRP on this mixed-features dataset and visualize using RadViz3D. Because of how our mixed-features datasets were generated, the MIXSIM-estimated pairwise overlaps between the 5 groups are essentially preserved (and displayed in the left columns of Fig. 1). Two views of RadViz3D displays of each dataset are in the middle two columns, and a 3D UMAP [12] visualization is in the right column of Fig. 1). Fig. S1 provides interactive

3D displays of RadViz3D, UMAP, t -SNE, Viz3D, and star coordinate plots with OLDA and ULDA. (OLDA, ULDA and MRP assume a low-dimensional linear subspace and require continuous variables while the default Euclidean distance used by UMAP and t -SNE is not always appropriate for mixed-features data. These methods are all also scale-variant. We use the GDT in mixed-features datasets – itself a major contribution of the paper – to address all these issues in all methods.) Further, in discussing the different displays, we note that the objective behind accurate visualization of labeled data is the display of labels according to the actual separation between them.

Fig. 1 and Fig. S1 show that Radviz3D provides meaningful displays that track the difficulty of separation very well as $\tilde{\omega}$ increases from 0.001 through 0.01 to 0.05 (see Fig. S1 for dynamic displays for $\tilde{\omega} \in \{0.0001, 0.001, 0.01, 0.05, 0.25\}$). Further, Fig. 1a shows the highest overlap between Groups 3 and 5 and between Groups 1 and 2 is fairly accurately reproduced in the RadViz3D display. Similar patterns are also noticed in Figs. 1b and 1c. For instance, in Fig. 1b, there are high overlaps between Groups 2 and 4 and between Groups 2 and 5, and these high overlaps, relative to the other pairs, is also reflected in the RadViz3D display. From Fig. 1c, we see that Groups 2 and 4 have the highest overlap and again RadViz3D produces a display consistent with this observation. Our illustrative experiment therefore shows RadViz3D's ability to faithfully display high-dimensional grouped datasets with varying separation. Our displays of the competing methods show that, but for UMAP, they are unable to display the separation of classes even in the case when they are generated with low $\tilde{\omega}$. UMAP (for instance, Fig. 1 can separate out classes in all cases very well, but can not distinguish the cases when class labels are well-separated from the cases when they are not. Specifically, UMAP provides similar representation of the distinctiveness of the groups across all cases regardless of whether the groups are well- or poorly-separated (as quantified by the overlap measures). We contend that this good separation of data by labels regardless of their overlap or difficulty of separation is a desirable property of a classification algorithm but not for visualization which should faithfully render the correct status and should display well-separated labeled data as such and poorer-separated labeled data as such. In that goal, only RadViz3D provides meaningful displays.

IV. REAL-DATA EXAMPLES

We now explore the visualization of datasets with continuous, discrete or mixed features. The focus of our work is on displaying high-dimensional datasets, so we provide only one moderate (9D) example. Our other examples have larger p , in some cases of several thousands. For brevity, we only have static displays here with RadViz3D, and refer to the online resource for dynamic or competing displays.

A. Datasets with discrete features

We begin with datasets with discrete features. There exist no competing methods that can handle such datasets so we use the GDT on these datasets before using them. The MRP

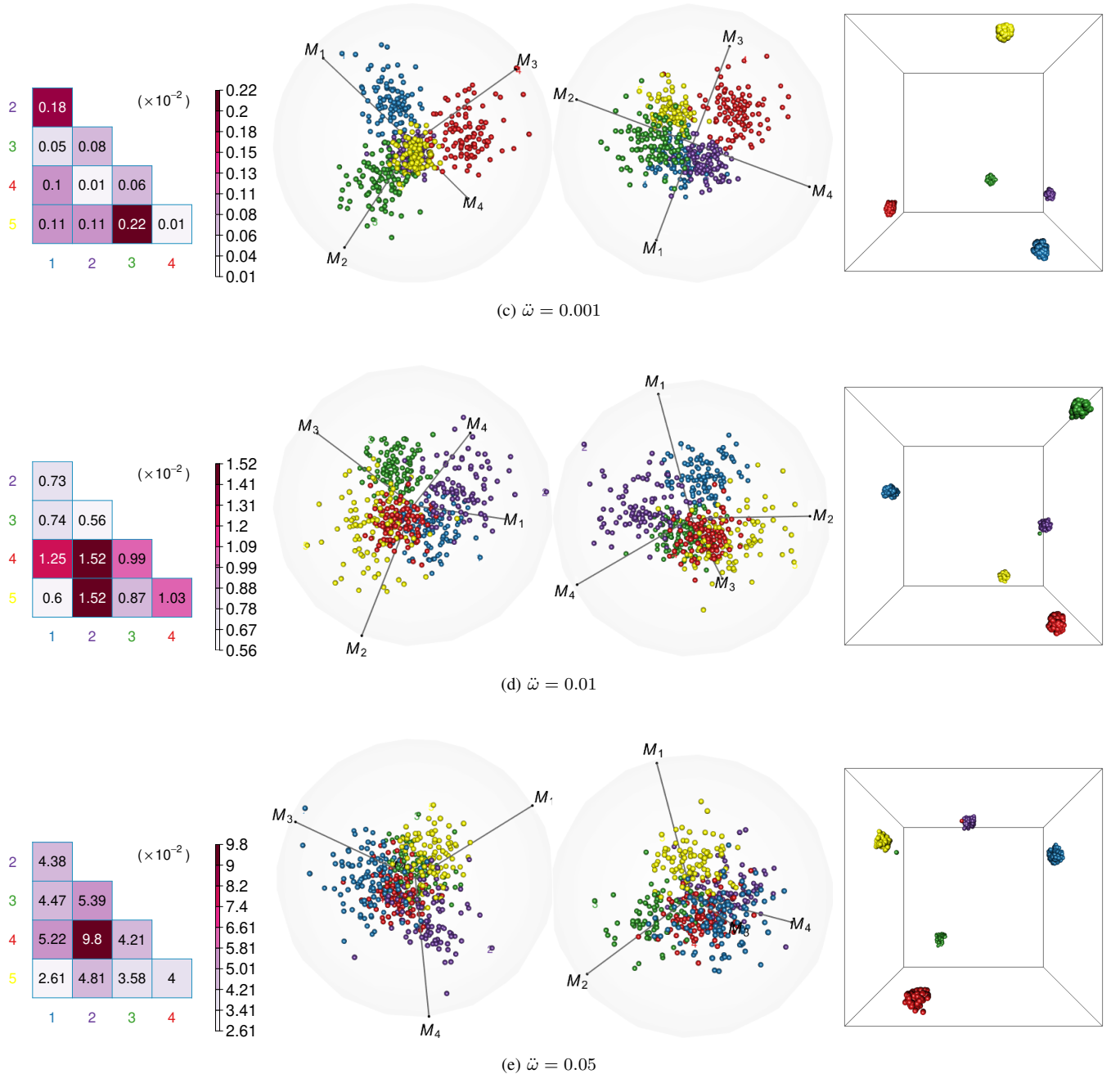


Fig. 1: Overlap maps (Ω , left) RadViz3D (middle figures) and UMAP displays (right) of simulated 100D mixed-feature datasets of varying group separation ($\tilde{\omega}$). Label colors in Ω match those in the RadViz3D displays.

is also used before displaying with RadViz3D, star coordinates and Viz3D displays.

1) *Voting records of US senators*: The 108th US Congress had 55 Republican and 45 Democratic (including 1 independent in the Democratic caucus) senators vote on 542 bills [29]. We display the senators according to whether they voted for each bill or not (*i.e.* against/abstained). The RadViz3D (Fig. 2, Fig. S6f) display distinguishes the 2 groups, reflecting the political affiliation. Here $G = 2$, so three zero-eigenvalue projections beyond the MRP are used in the RadViz3D display. As explained in Section II-B0b, these additional projections (associated with the anchor points X_2, X_3, X_4) do not con-

tribute towards separating the two groups which are separated solely by the first MRP (associated with X_1). A physical interpretation is that the spring on anchor point X_1 pulls one group harder than another group, separating it out, while the “null” springs on X_2, X_3, X_4 pull both groups with equal force. All anchor points are evenly-distributed on the unit sphere, so the forces applied by X_2, X_3, X_4 cancel and only the spring attached to X_1 separates the first group from the second in the visualization. RadViz3D and UMAP separate out the two groups, but RadViz3D, unlike UMAP (Fig. S6b), also gives us a sense of the closeness of some senators in either group with the other. The t -SNE (Fig. S6a), Viz3D (Fig. S6e)

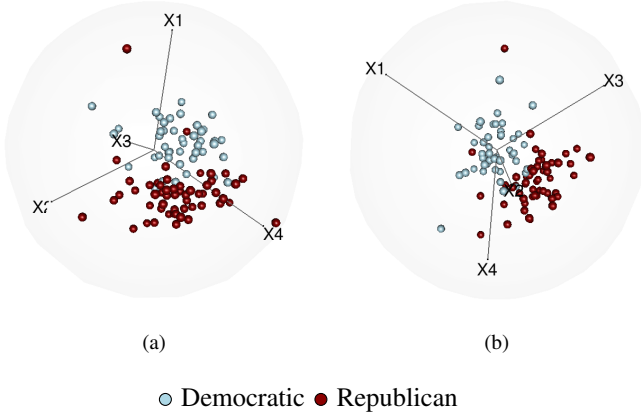


Fig. 2: RadViz3D displays of senators' voting records.

and especially star coordinate plots with ULDA (Fig. S6c) and OLDA (Fig. S6d) are unable to separate the two parties.

2) *Adult Autism Spectrum Disorder (ASD) screening*: This dataset [30] from the UCI's Machine Learning Repository (MLR) [31] has 15 binary (and 5 additional) features on 515 normal and 189 ASD-diagnosed adults. The two groups

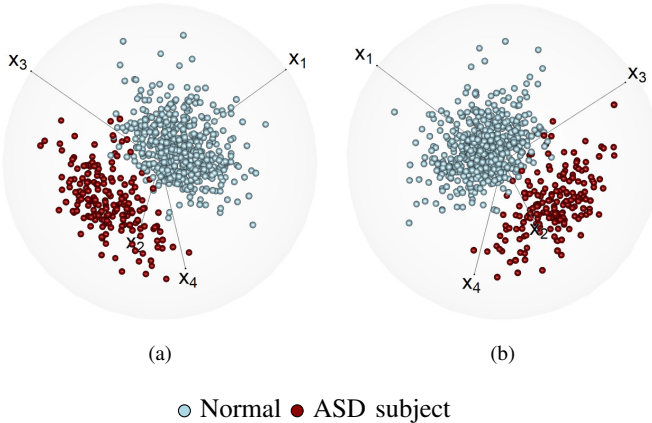


Fig. 3: RadViz3D displays of the ASD screening dataset.

are reasonably well-separated, with minimum classification error of 1.7% [32], and therefore should be easily separated. RadViz3D (Fig. 3 and Fig. S7f) performs better in separating two groups than t -SNE (Fig. S7a), star coordinates with OLDA (Fig. S7c) or ULDA (Fig. S7d), and Viz3D (Fig. S7e). UMAP (Fig. S7b) also separates the two groups, but they are completely disjoint and does not accurately reflect the best misclassification rate of 1.7% for this dataset.

3) *SPECT heart dataset*: This dataset [33] from the UCIMLR [31] has 22 binary attributes that summarize cardiac Single Proton Emission Computed Tomography (SPECT) images of 55 normal and 212 abnormal patients. Each image was summarized by means of 44 continuous features that was further processed to obtain 22 binary features [33]. The separation between these two groups is very good with current classification results [34] finding small but positive misclassification rates. In this example, RadViz3D (Fig. 4 and Fig. S8f) performs well in separating the two groups with very small overlap. UMAP (Fig. S7b) again produces disjoint groups in

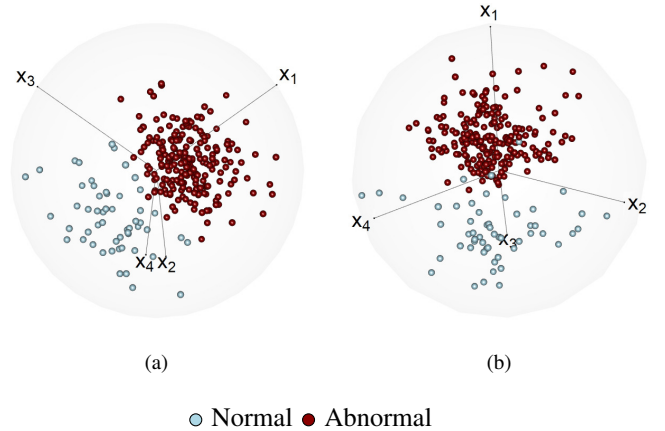


Fig. 4: RadViz3D displays of the SPECT Heart dataset.

the visualization and fails to accurately reflect the non-zero misclassification rate between the two groups while t -SNE (Fig. S8a), Viz3D (Fig. S8e) and especially star coordinate plots with OLDA (Fig. S8c) or ULDA (Fig. S8d) fail to clearly display the separability of the two groups.

B. Datasets with mixed features

We now illustrate performance of RadViz3D on two real datasets with continuous and discrete-valued features. No method can currently display such datasets, so as in Section IV-A, we employ the GDT (and the MRP for RadViz3D and Viz3D) on the datasets before their display.

1) *Indic scripts*: This dataset [35] is on 116 different features from handwritten scripts of 11 Indic languages. We choose a subset of 5 languages from 4 regions, namely Bangla (from the east), Gurmukhi (north), Gujarati (west), Kannada and Malayalam (languages from the neighboring southern states of Karnataka and Kerala) and a sixth language (Urdu, with a distinct Persian script). Figure. 5a displays a line from a sample document in each script and illustrates the challenges in characterizing handwritten scripts because of the additional effect of individual handwriting styles. The challenges of accounting for handwriting variability, and the distinctiveness of the six scripts are captured well in the RadViz3D displays (Figs. 5b, 5c and S9f). For example, we see that Kannada and Malayalam are close by in the displays. The three Sanskrit-based languages of Bangla, Gujarati and Gurmukhi are neighbors of each other in the displays. The placement of Urdu farther from the rest but still close to both Gujarati and Bangla indicates the possible influence of Persian, for reasons of history and geography, on the handwriting of these scripts. The RadViz3D displays therefore make intuitive sense for this dataset. The t -SNE (Fig. S9a) and UMAP (Fig. S9b) displays distinguish the scripts very well but do not depict similarities between them. Indeed, the UMAP display separates even individuals from within the scripts, and in our view, performs poorly. Viz3D (Fig. S9e) distinguishes Urdu, Kannada and Gujarati very well but not the other languages while star coordinate plots (Figs. S9c,d) with OLDA and ULDA do poorly.

REFERENCES

- [1] S. K. Card, J. D. Mackinlay, and B. Schneiderman, *Readings in information visualization: using vision to think*. Morgan Kaufmann, 1999.
- [2] E. Bertini, A. Tatu, and D. Keim, "Quality metrics in high-dimensional data visualization: an overview and systematization," *IEEE Transactions on Visualization and Computer Graphics*, vol. 17, no. 12, p. 2203–2212, 2011.
- [3] J. M. Chambers, W. S. Cleveland, B. Kleiner, and P. A. Tukey, *Graphical Methods for Data Analysis*. Belmont, CA: Wadsworth, 1983.
- [4] H. Chernoff, "The use of faces to represent points in k-dimensional space graphically," *Journal of the American Statistical Association*, vol. 68, no. 342, pp. 361–368, 1973.
- [5] A. Inselberg, "The plane with parallel coordinates," *The Visual Computer*, vol. 1, pp. 69–91, 1985.
- [6] E. Wegman, "Hyperdimensional data analysis using parallel coordinates," *Journal of the American Statistical Association*, vol. 85, pp. 664–675, 1990.
- [7] U. Fayyad, G. Grinstein, and A. Wierse, *Information Visualization in Data Mining and Knowledge Discovery*. Morgan Kaufmann, 2001.
- [8] D. F. Andrews, "Plots of high-dimensional data," *Biometrics*, vol. 28, no. 1, pp. 125–136, 1972.
- [9] R. Khattree and D. N. Naik, "Andrews plots for multivariate data: Some new suggestions and applications," *Journal of Statistical Planning and Inference*, vol. 100, no. 2, pp. 411–425, 2002.
- [10] K. R. Gabriel, "The biplot graphical display of matrices with application to principal component analysis," *Biometrika*, vol. 58, pp. 453–467, 1971.
- [11] E. Kandogan, "Visualizing multi-dimensional clusters, trends, and outliers using star coordinates," in *Proceedings of the Seventh ACM SIGKDD International Conference on Knowledge Discovery and Data Mining*, ser. KDD '01. New York, NY, USA: ACM, 2001, pp. 107–116. [Online]. Available: <http://doi.acm.org/10.1145/502512.502530>
- [12] L. McInnes, J. Healy, N. Saul, and L. Grossberger, "Umap: Uniform manifold approximation and projection," *Journal of Open Source Software*, vol. 3, p. 861, 09 2018.
- [13] P. Hoffman, G. Grinstein, K. Marx, I. Grosse, and E. Stanley, "DNA visual and analytic data mining," in *Proceedings of the 8th conference on Visualization '97, VIS'97*. IEEE Computer Society Press, 1997, p. 437–441.
- [14] P. Hoffman, G. Grinstein, and D. Pinkney, "Dimensional anchors: a graphic primitive for multidimensional multivariate information visualizations," in *Proceedings of the 1999 workshop on new paradigms in information visualization and manipulation in conjunction with the eighth ACM international conference on Information and knowledge management*. ACM, 1999, pp. 9–16.
- [15] G. G. Grinstein, C. B. Jessee, P. E. Hoffman, P. J. O'Neil, and A. G. Gee, "High-dimensional visualization support for data mining gene expression data," in *DNA Arrays: Technologies and Experimental Strategies*, E. V. Grigorenko, Ed. Boca Raton, Florida: CRC Press LLC, 2001, ch. 6, pp. 86–131.
- [16] G. M. Draper, Y. Livnat, and R. F. Riesenfeld, "A survey of radial methods for information visualization," *IEEE Transactions on Visualization and Computer Graphics*, vol. 15, no. 5, pp. 759–776, Sep. 2009.
- [17] A. O. Artero and M. C. F. de Oliveira, "Viz3d: effective exploratory visualization of large multidimensional data sets," in *Proceedings. 17th Brazilian Symposium on Computer Graphics and Image Processing*, Oct 2004, pp. 340–347.
- [18] Y. Zhu, F. Dai, and R. Maitra, "Fully three-dimensional radial visualization," 2021.
- [19] L. Rüschemdorf, *Mathematical Risk Analysis*. Berlin Heidelberg: Springer-Verlag, 2013.
- [20] Y. Benjamini and Y. Hochberg, "Controlling the false discovery rate: a practical and powerful approach to multiple testing," *Journal of the Royal Statistical Society*, vol. 57, pp. 289–300, 1995.
- [21] Y. Koren and L. Carmel, "Robust linear dimensionality reduction," *IEEE Transactions on Visualization and Computer Graphics*, vol. 10, no. 4, pp. 459–470, July 2004.
- [22] G. Golub, C. Van Loan, C. Van Loan, and P. Van Loan, *Matrix Computations*, ser. Johns Hopkins Studies in the Mathematical Sciences. Johns Hopkins University Press, 1996. [Online]. Available: <https://books.google.com/books?id=mlOa7wPX6OYC>
- [23] J. Ye, "Characterization of a family of algorithms for generalized discriminant analysis on undersampled problems," *Journal of Machine Learning Research*, vol. 6, no. 4, 2005.
- [24] Z. Jin, J.-Y. Yang, Z.-S. Hu, and Z. Lou, "Face recognition based on the uncorrelated discriminant transformation," *Pattern recognition*, vol. 34, no. 7, pp. 1405–1416, 2001.
- [25] V. Melnykov, W.-C. Chen, and R. Maitra, "MixSim: An R package for simulating data to study performance of clustering algorithms," *Journal of Statistical Software*, vol. 51, no. 12, pp. 1–25, 2012. [Online]. Available: <http://www.jstatsoft.org/v51/i12/>
- [26] R Development Core Team, "R: A language and environment for statistical computing," R Foundation for Statistical Computing, Vienna, Austria, 2018, ISBN 3-900051-07-0. [Online]. Available: <http://www.R-project.org>
- [27] R. Maitra and V. Melnykov, "Simulating data to study performance of finite mixture modeling and clustering algorithms," *Journal of Computational and Graphical Statistics*, vol. 19, no. 2, pp. 354–376, 2010.
- [28] V. Melnykov and R. Maitra, "CARP: Software for fishing out good clustering algorithms," *Journal of Machine Learning Research*, vol. 12, pp. 69 – 73, 2011.
- [29] O. Banerjee, L. E. Ghaoui, and A. d'Aspremont, "Model selection through sparse maximum likelihood estimation for multivariate gaussian or binary data," *Journal of Machine Learning Research*, vol. 9, pp. 485–516, 2008.
- [30] F. Thabtah, "Autism spectrum disorder screening: machine learning adaptation and DSM-5 fulfillment," in *Proceedings of the 1st International Conference on Medical and Health Informatics 2017*. ACM, 2017, pp. 1–6.
- [31] D. J. Newman, S. Hettich, C. L. Blake, and C. J. Merz, "UCI repository of machine learning databases," 1998. [Online]. Available: [http://www.ics.uci.edu/\\$\sim\\$smlearn/MLRepository.html](http://www.ics.uci.edu/\simsmlearn/MLRepository.html)
- [32] S. Raj and S. Masood, "Analysis and detection of autism spectrum disorder using machine learning techniques," *Procedia Computer Science*, vol. 167, pp. 994–1004, 2020, international Conference on Computational Intelligence and Data Science.
- [33] L. A. Kurgan, K. J. Cios, R. Tadeusiewicz, M. R. Ogiela, and L. S. Goodenday, "Knowledge discovery approach to automated cardiac SPECT diagnosis," *Artificial Intelligence in Medicine*, vol. 23, no. 2, pp. 149–169, 2001.
- [34] S. S. Yadav, S. M. Jadhav, R. G. Bonde, and S. T. Chaudhari, "Automated cardiac disease diagnosis using support vector machine," in *2020 3rd International Conference on Communication System, Computing and IT Applications (CSCITA)*, 2020, pp. 56–61.
- [35] S. M. Obaidullah, C. Halder, K. C. Santosh, N. Das, and K. Roy, "Phindic_11: page-level handwritten document image dataset of 11 official indic scripts for script identification," *Multimedia Tools and Applications*, vol. 77, no. 2, pp. 1643–1678, Jan 2018. [Online]. Available: <https://doi.org/10.1007/s11042-017-4373-y>
- [36] Q. Wang, J. Armenia, C. Zhang, A. Penson, E. Reznik, L. Zhang, T. Minet, A. Ochoa, B. Gross, C. A. Iacobuzio-Donahue, D. Betel, B. S. Taylor, J. Gao, and N. Schultz, "Unifying cancer and normal RNA sequencing data from different sources," *Scientific Data*, vol. 5, p. 180061, 04 2018.